# Physical Insights on the Ambiguous Metal–Graphene Interface and Proposal for Improved Contact Resistance

Mayur Ghatge and Mayank Shrivastava, *Member, IEEE*

***Abstract*— The ambiguous behavior of metal–graphene interface has been addressed in this paper using density functional theory and nonequilibrium Green's function formalism. For the first time, the fundamental chemistry of metal–graphene interface, in particular role of sp-hybridized and $sp^2$-hybridized carbon atoms, has been emphasized and discussed in detail in this paper. It was discovered that the sp-hybridized sites at the edge of a graphene monolayer contribute to 40% of current conduction when compared with $sp^2$-hybridized atom sites in the graphene–metal overlap region. Moreover, we highlighted the insignificance of an additional metal layer, i.e., sandwiched contact, due to lacking sp-hybridized carbon sites. A fundamental way of defining the contact resistance, while keeping chemical bonding in mind, has been proposed. The bonding insight has been further used to propose the novel ways of interfacing metal with graphene, which results in a 40% reduction in contact resistance.**

***Index Terms*— Chemical bonding, contact resistance, edge contacts, graphene, metal–graphene interface, palladium–graphene interface.**

## I. Introduction

GRAPHENE with its unique and superior properties [1]–[5] is expected to play a vital role in emerging nanoelectronics and RF applications. This is evident from the estimated (theoretically) cutoff frequencies of 2–20 THz [6], [7]. However, the highest cutoff frequency ($f_T$), experimentally reported until now is 427 GHz [8], which shows a big gap between expected performance and state of the art. One of the major hindrance in realizing terahertz graphene FET is the contact resistance ($R_c$), i.e., weak metal–graphene interface.

A number of experimental work, to lower the metal–graphene contact resistance, have been widely reported until now. However, investigations often fail to explain the root cause behind the high contact resistance or the shown improvements are misleading in nature. For example, Yu *et al.* [9] have proposed the graphene work function tuning using a back-gate electric field to lower the graphene–metal contact resistance. However, the explanation is limited to work function difference and lowering of barrier height with the application of an electric field. Studies of metal–graphene standard overlapping contacts and standard edge contacts have been done excessively [10]–[15]. The overlapping contacts were shown to have higher contact resistance when compared with the edge contacts [12]–[15]. An improved metal–graphene interface due to in-plane contacts in the edge-contacted structure is attributed to the reduction in contact resistance. However, the first-principle analysis of the edge contacts and atomic-scale comparison of the edge contacts with overlapping contacts have never been analyzed in detail. This manuscript reveals a more fundamental mechanism leading to this improved contact resistance, which is missing in earlier works. Franklin *et al.* [16] have shown that the double-sided (sandwiched) contact geometry can lower the contact resistance by 40% when compared with standard overlapping contacts. Franklin *et al.* [16] have attributed this to the improved coupling between metal and graphene; however, they have failed to account for process lead differences and die-to-die variations. Moreover, the physical insights leading to this improvement are also missing in the earlier works. In this paper, we demonstrate using density functional theory (DFT) and nonequilibrium Green's function (NEGF) formalism that sandwiched contacts do not improve the contact resistance as proposed in [16].

Stokbro *et al.* [17] have reported the theories related to current flow at the nickel–graphene interface. However, the current flow and voltage drop mechanism at the palladium–graphene interface and other related interfaces is missing in the literature. For example, how changing the metal with the lower work function than graphene affects the voltage drop? Frederiksen *et al.* [18] have used the first-principle analysis to explain the impact of an electrode metal on transport characteristics of metal–$sp^2$ carbon interface using a single $C_{60}$ molecule. Still carrier transport through $sp^2$ graphene sheet and sp-hybridized graphene edge, when interfaced with metal are by and large open questions. Moreover, further clarity on the current pathways and the role played by the sp-hybridized carbon atoms over the interface properties is highly desired. Robinson *et al.* [19] have reported how $O_2$-plasma etching and subsequent thermal annealing with varying annealing time can improve the value of the contact resistance by forming a high quality interface. Leong *et al.* [20] explain how thermal annealing unknowingly creates defects

Manuscript received May 27, 2015; revised July 24, 2015; accepted September 21, 2015. Date of publication October 8, 2015; date of current version November 20, 2015. This work was supported by the Department of Science and Technology, Government of India, under Project SB/S3/EECE/063/2014. The review of this paper was arranged by Editor M. S. Bakir.

The authors are with the Advanced Nanoelectronic Device and Circuit Research Laboratory, Department of Electronic Systems Engineering, Indian Institute of Science, Bangalore 560012, India (e-mail: mayank@dese.iisc.ernet.in).

Color versions of one or more of the figures in this paper are available online at http://ieeexplore.ieee.org.

Digital Object Identifier 10.1109/TED.2015.2481507

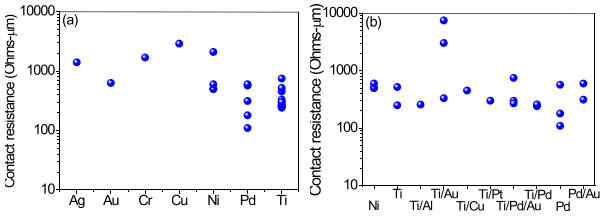


Fig. 1. (a) Contact resistance ($R_c$) comparison for different metal–graphene interfaces. (b) Comparison of contact resistance ($R_c$) for different metal stacks interfaced with the graphene and palladium–graphene interface.

in the graphene sheet and forms edge contacts within the contact region which in turn reduces the contact resistance. These defects improve the value of $R_c$, which is also seconded in [21]. Finally, the fundamental chemistry behind the contact resistance improvement by the creation of defects in the graphene sheet is open for deeper explorations.

This paper addresses the following open questions and is arranged as follows. Section II describes the computational setup used for the first-principle analysis and gives reasoning for the selection of metal in this paper. Chemical role of the metal–graphene interface, in particular role of sp-hybridized and $sp^2$-hybridized carbon atoms, is discussed in Section III. Section IV addresses the anomalous behavior of the graphene–metal interface, whereas the relative contribution of an edge region in lowering the contact resistance is addressed in Section V. Novel ways of interfacing metal with graphene have been proposed in Section VI. Finally, this paper is concluded in Section VII.

## II. Computational Setup

Until now various metals [22] have been used to form an ohmic contact with graphene. Palladium (Pd), nickel (Ni), chromium (Cr), and titanium (Ti) are reported to form a strong bond with graphene [22]; however, improved bonding may not always result into the reduced contact resistance. Moreover, often wetting metal layers have also been used to improve the transport efficiency of the metal–graphene interface. Fig. 1 summarizes the contact resistance values reported for various different metal/metal-stacks with the graphene sheet. Palladium has been reported to have the lowest contact resistance with graphene. Keeping this in mind, palladium has been used for the computational studies in this paper.

The palladium–graphene contact structure's cross-sections are shown in Fig. 2. The simulation domain is virtually divided into three regions, namely edge, overlap, and channel regions, for the sake of clear explanations, as shown in Fig. 2(a). It is worth highlighting that, in order to form an interface with least lattice mismatch between palladium and graphene, palladium is cleaved across all directions before forming an interface with graphene. Moreover, Pd(111) is used for analysis, as the lattice mismatch between Pd(111) and graphene is the least (∼2%). However, the strain effects due to finite lattice mismatch have been considered for a few initial simulation for completeness [Fig. 2(b)]. In addition to these, a standard edge structure [Fig. 2(c)] as well as a sandwiched structure [Fig. 2(d)] is also analyzed for the completeness of insights presented. In this paper, a zigzag edge of the graphene is directed along the transport direction and an armchair edge in the overlap region. It is worth highlighting that the findings in this paper are expected to be independent of edge type along the transport direction. This is attributed in [17], which explains that the contact resistance remains independent of the edge type in the transport direction. *Ab-initio* DFT and NEGF formalisms are used for the calculations and analysis [23], [24], while using QuantumWise ATK simulation package for this paper [25]. The local density approximation describes the exchange-correlation interaction between the electrons. The density mesh cutoff is 75 Hartee (150 Rydberg) with 12 k-points in the direction of structure's periodicity. Furthermore, a Poisson solver that combines a fast Fourier transform method in the transverse transport direction (direction in which a structure is periodic), while a multigrid Poisson solver in the transport direction (using a Dirichlet boundary condition) has been used for this paper. A source–drain bias of 250 mV is applied to conduct the carrier transport analysis. Finally, the calculations are done for electron temperature of 300 K using a single-zeta polarized basis set for palladium as well as carbon atoms.

## III. Chemical Role at Palladium–Graphene Contact

Carbon with its electronic configuration of $\{1s^2 2s^2 2p^2\}$ has two electrons in its s and p orbitals ($p_x$ and $p_y$ each). These s, $p_x$, and $p_y$ orbitals combine to form directional sigma bonds with three neighboring carbon atoms in the plane and create an $sp^2$-hybridized orbital. The $p_z$ orbital of carbon atoms together form a cloud of $\pi$-electrons resulting in a resonating $\pi$ bond [26]. These resonating $\pi$-electrons and sigma bonds lead to unique and superior electrical and mechanical properties. With $sp^2$-hybridization, carbon achieves an electronic configuration of $\{1s^2 2s^2 2p^6\}$ which is the same as the next noble element neon (Ne). As there are no empty/half-filled d orbitals in carbon, there is no possibility for the carbon atoms in the graphene sheet to interact chemically with metal atoms. Unlike the carbon atoms in the interiors, the carbon atoms at the edges are sp-hybridized which, in general, have potential to form much stronger chemical bond with transition metals compared with $sp^2$-hybridized carbon atoms [27].

As carbon is more electronegative than palladium, the electron cloud in the Pd–carbon covalent bond is inclined toward the carbon atom. For carbon atoms in the three regions [Fig. 2(a)], Fig. 3 shows the charge transfer from palladium to carbon. We observe that a substantial charge transfer of the order of ∼0.1 e per C atom from palladium to carbon at the edge region; however, the same in the overlap region is ∼0.06 e per C atom. Moreover, the charge transfer from Co and Ni atoms to C has earlier been reported to be 0.05 e and 0.07 e per C atom, respectively, [28]. These observations manifest the following: 1) high bond strength between Pd and graphene at the edge region when compared with the overlap region; 2) high bond strength between Pd and graphene when compared with other metals; 3) the edge region may offer a less resistance path when compared with the overlap region; and 4) the bonding between metal and

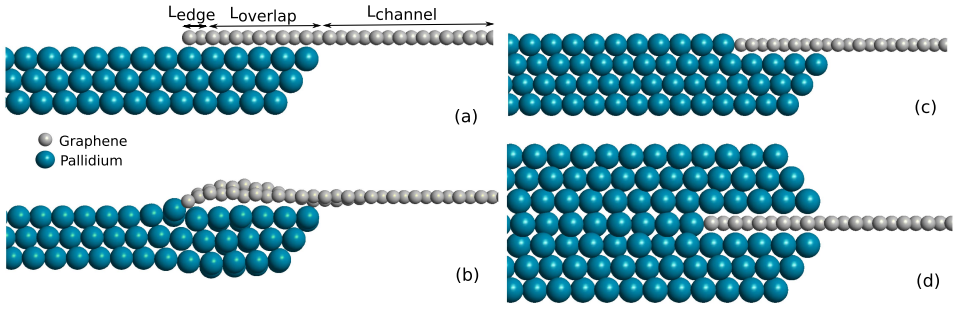


Fig. 2. Pd(111) is interfaced with zigzag graphene edge along the transport direction. The channel length used in each case is ∼90 Å and bias between graphene and palladium ends is 250 mV. Front view of (a) standard overlapping-contact structure, (b) relaxed overlapping-contact structure, (c) standard edge-contact structure, and (d) sandwich-contact structure.

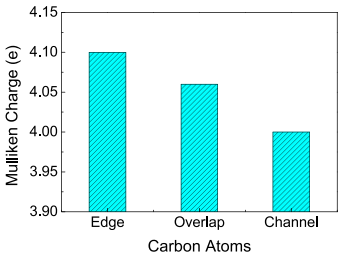


Fig. 3. Mulliken charge population of carbon atoms in the edge, overlap, and channel regions of the graphene.

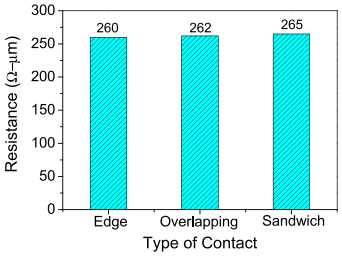


Fig. 4. Resistance (in $\Omega\mu$m) for edge-contact, standard overlapping-contact, and sandwich-contact structures for the graphene channel length of ∼90 Å and bias between graphene and palladium ends is 250 mV.

graphene plays a critical role in defining the contact properties and, therefore, a deeper understanding of the contact chemistry is required.

## IV. Anomalous Graphene–Metal Contacts

An edge contact, as shown in Fig. 2(c), has been demonstrated earlier to have the reduced contact resistance when compared with an overlapping-contact geometry [Fig. 2(a)] [12]–[15]. This behavior is assumed to be attributed to the formation of strong chemical covalent bonds between the graphene and metal atoms. In addition to an edge contact, a double-side contact (or sandwiched contact), as shown in Fig. 2(d), was experimentally demonstrated to reduce the contact resistance by ∼40% in [16]. This behavior was also assumed to be attributed to: 1) enhanced graphene–metal coupling/bonding and 2) increased graphene doping in the presence of top as well as bottom metal layers [16]. We suspect that the improvements reported in [16] might be due to process artifacts or variations. For example, processes, such as annealing and plasma ashing, do introduce basal defects within the graphene sheet. Such defects can improve the contact resistance as discussed later in this paper. Our investigations, as presented in this section, show a different and anomalous behavior when compared with earlier works. Moreover, a detailed atomistic picture of molecular bonding leading to the contact resistance improvement in the edge and sandwiched geometries is missing in these works, which is addressed in this paper.

Fig. 4 shows that the contact resistance remains by and large unchanged for various contact geometries, as shown in Fig. 2. The difference in the resistance value is <2% (Fig. 4). Interestingly, the resistance of the sandwiched contact is 2% higher than the standard contact, unlike in [16]. This behavior can be attributed to the limited empty orbitals present at the graphene edge for bonding with metal atoms. This hypothesis is investigated in detail in this section. The overlapping-contact geometry with the palladium–graphene distance of ∼2.2 Å forms a stable bond with $p_z$–$d_{z^2}$ orbitals. To understand the bonding phenomenon, the overlapping-contact geometry [Fig. 2(a)] is relaxed, so that the maximum force in the structure is <0.05 eV/Å. The relaxed structure [Fig. 2(b)] displays how the graphene loses its planar nature at the edge of the interface and also that the palladium atoms are pinned up to a graphene layer and lifted from their actual position. Palladium has an electronic configuration of $\{[Ar]4d^{10}5s^0\}$ in the ideal state. But, as the 5s and 4d orbitals have nearly the same energy, electrons from 4d orbitals are excited easily to the 5s orbital. The 4d orbital ($d_{z^2}$) then overlaps with the $p_z$ orbital of carbon to form a strong covalent bond. The relaxed structure shows that the edge-geometry [Fig. 2(b)] is not a binding factor to form a stable strong chemical bond.

To investigate the phenomenon at the interface of the edge-contacted geometry as well as the sandwiched geometry, we analyzed the local density of states (LDOS) for both the structures and compared them with the LDOS of the overlapping-contact structure. A edge-contact structure [Fig. 5(b)] as well as a sandwiched structure [Fig. 5(c)] shows increased DOS for energies lower than 0 eV when compared with the standard overlapping-contact structure [Fig. 5(a)]. However, this improvement is attributed to increased DOS of palladium

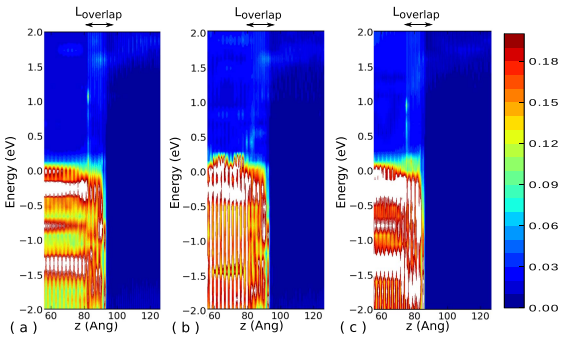


Fig. 5. LDOS for (a) standard overlapping-contact structure, (b) edge-contact structure, and (c) sandwich-contact structure. The LDOS is averaged along the width of the palladium–graphene-contacted structures (the regions marked in white are beyond the scale).

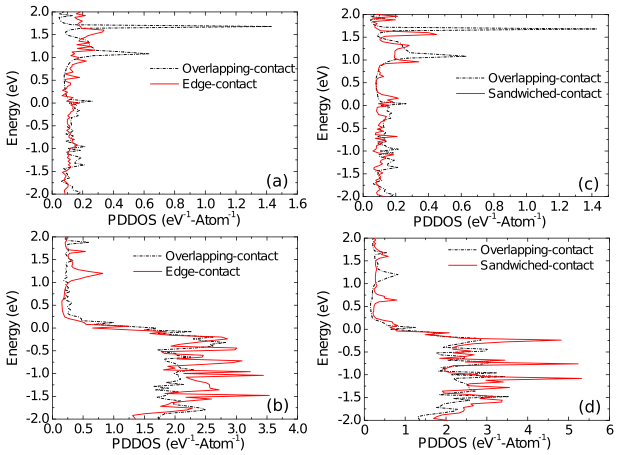


Fig. 6. PDDOS in standard overlapping and edge-contacted structures for (a) graphene in the interface region and (b) palladium in the interface region. PDDOS in standard overlapping-contact and sandwiched-contact structures for (c) graphene in the interface region and (d) palladium in the interface region.

as evident from Fig. 6. Projected device density of states (PDDOS) for the graphene at the interface is shown in Fig. 6(a) and (c) while Fig. 6(b) and (d) shows the PDDOS for palladium atoms at the interface. For energies lower than 0 eV, the PDDOS for graphene does not vary for edge as well as sandwiched structures when compared with the overlapping structure, while the PDDOS for palladium is increased for the edge-contact and sandwiched structures when compared with the overlapping-contact structure. The unaffected DOS of graphene further justifies the indifference in the resistance values.

Difference in the charge distribution at the interfaces of the edge and overlapping structures was studied further using the electron difference density (EDD) (Fig. 7) in the graphene plane. The EDD is defined as the difference between the electron valence density and the neutral atom electron density along the transport direction. The EDD in overlapping contact [Fig. 7(a)] does not vary much from the edge-contacted structure [Fig. 7(b)]. A spike in the edge structure [Fig. 7(b)] at the fractional coordinate 0.47 (edge region of the contact) shows the slight difference in the charge rearrangement at the palladium–graphene interface edge. This spike explains

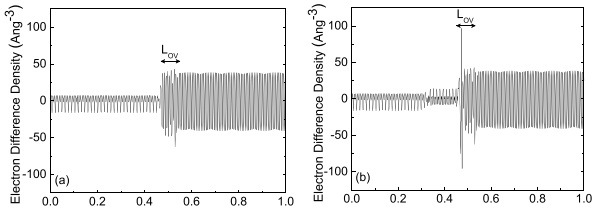


Fig. 7. EDD for (a) overlapping-contact structure and (b) edge-contact structure plotted along the transport direction with length in fractional coordinates. $L_{ov}$ is marked as the overlap region length in standard overlapping and edge-contacted structures.

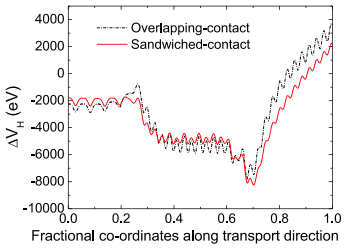


Fig. 8. Electrostatic difference potential of overlapping-contact and sandwich-contact structures plotted along the transport direction with length in fractional coordinates.

the slight improvement in charge distribution due to edge contact geometry when compared with the overlapping-contact geometry. We can, hence, conclude that irrespective of the edge or overlapping-contact structure, as palladium forms a strong covalent bond with unhybridized carbon atoms, the difference in the contact resistance is negligibly small. This difference might be relatively higher for metals with weak tendency to form bonds with graphene. Thus, modification in the edge contact interfacing technique does not reduce the resistance for metals having high tendency to form covalent bonds.

On one hand, the discussion above justifies that new methods to further reduce the contact resistance must be discovered and exploited. However, on the other hand, the 2% higher resistance of sandwiched contact unlike reported earlier [16] remains a mystery. To address the indifference between the overlapping-contact structure and sandwiched structures, electrostatic difference potential [$\Delta V_H$(eV)] across both the structures along the transport direction (in fractional co-ordinates), as shown in Fig. 8, is compared. As the work function of graphene is higher than that of palladium, electron transfer from palladium to graphene can be seen, which leads to rising of electrostatic potential within graphene. Fig. 8 shows the unchanged electrostatic potential for the overlapping-contact structure and sandwiched structures in the interface region ($0.25 < x < 0.6$), which suggests why the sandwiched structures do not change the contact property and, hence, may not help in reducing the contact resistance.

Finally, it is worth investigating the carrier transport behavior across the overlapping-contact, sandwiched-contact, and edge-contact structures to validate our conclusions above. Fig. 9 compares the respective transmission spectrum [T(E)] and shows no significant change. This proves that the carrier transport channels remain intact and are independent of

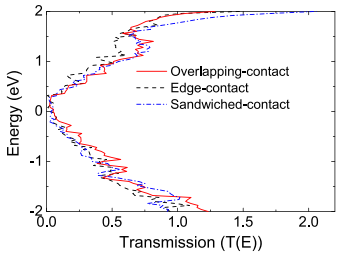


Fig. 9. Transmission spectrum of the edge-contacted [Fig. 2(c)], sandwiched-contacted [Fig. 2(d)], and overlapping-contacted [Fig. 2(a)] structures.

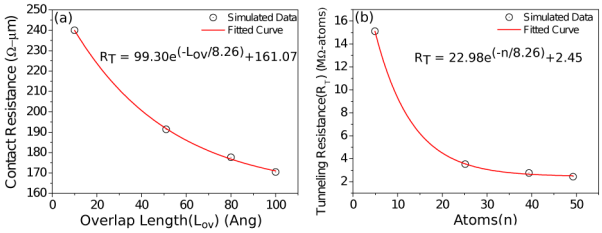


Fig. 10. Fitted curve and fitting function for (a) contact resistance (in $\Omega\mu$m) versus palladium–graphene overlap length ($L_{ov}$) and (b) tunneling resistance (in M$\Omega-atoms$) versus number of atoms ($n$) in the tunneling region.

edge or sandwiched geometry. To understand this anomalous behavior, one can dig into the orbital theory. As carbon atoms at the edge of the graphene sheet is sp-hybridized and the $\pi$-electrons are resonating in the plane, these carbon atoms at the edge can only form an additional sigma bond with the metal atoms as shown by the palladium–graphene relaxed structure [Fig. 2(c)]. Hence, the bonding channel remains invariant of the presence of single-sided or double-sided metal contacts. Thus, a sandwiched structure does not improve the chemical covalent bonding between palladium and graphene, causing no change in the contact resistance unlike suggested in [16]. In fact, for the sandwiched structure [Fig. 2(d)], a slight increase in resistance is observed, which can be attributed to the formation of chemical bond between some of the palladium atoms on either side of the graphene monolayer instead to the carbon atom in the graphene sheet.

## V. Edge Versus Overlap Resistance

One can recall from the anomalous graphene–metal contacts section that the carrier transport through the edge region is through the bonding channels, whereas the same from the overlap region is through the tunneling channels. This raises a fundamental question—what percentage of current flows through the sp-hybridized edge region and what through the sp$^2$-hybridized overlap region? In other words, what is the relative contribution of the edge region in lowering the contact resistance? To address this question, we have studied the contact resistance as a function of overlap length, as shown in Fig. 10(a). The edge region's contribution in lowering the contact resistance is extracted by extrapolating the characteristics presented in Fig. 10(a) to the overlap length of 0 Å. This ignores carrier transport contribution through the overlap region. We can think of extracted contact resistance ($R_c$) as a parallel combinations of edge and overlap

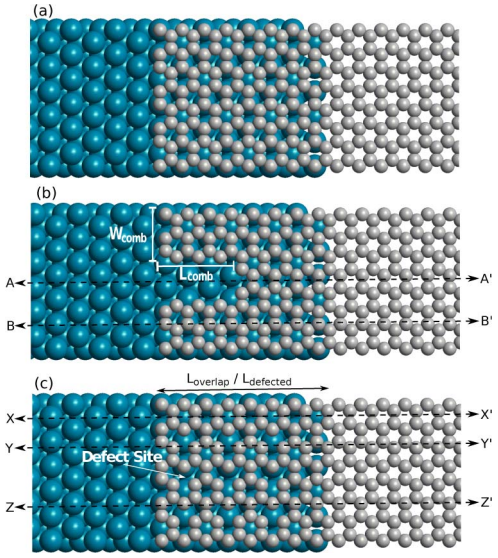


Fig. 11. Top view of (a) standard structure, (b) comb-shaped-contact structure, and (c) defected-contact structure. The cut-planes AA′, BB′, XX′, YY′, and ZZ′ are used to analyze the potential drop (Fig. 16).

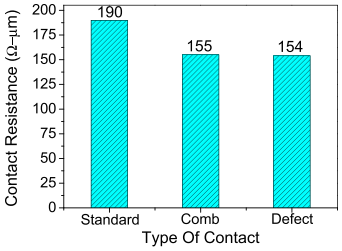


Fig. 12. Contact resistance (in $\Omega\mu$m) for standard structure, comb-shaped-contact structure, and defected (chemically bonded overlap) structure for 250 mV bias between palladium and graphene ends.

region's contact resistances ($R_e$ and $R_T$, respectively). This results in an edge region's resistance (which lowers the contact resistance by 40%) of $\sim$260 $\Omega\mu$m.

The other question one can think of is—is there even a more fundamental way of defining the contact resistance? For example, the contact resistance is dependent on the nature of transport and per unit atoms. We have transformed the edge and overlap region's contact resistances by multiplying the same with the number of carbon atoms present at the edge (sp-hybridized carbon atoms) and in the sp$^2$-hybridized overlap region. The former is calculated to be 1.28 M$\Omega-atoms_{\rm sp}$ and the latter is shown in Fig. 10(b) as a function of number of carbon atoms ($n$), in the units of M$\Omega-atoms_{\rm sp^2}$. It is worth highlighting that the extracted numbers may not be universal as it depends on various parameters, such as metal DOS, work-function, applied bias, and device width. Hence, further work is required to derive fundamental constants showing the contact behavior.

## VI. Proposal for Contact Resistance Improvement

The chemical role of sp-hybridized carbon atoms at the edge suggests that increasing the sp-hybridized sites can potentially improve the contact resistance. These chemical bonding sites

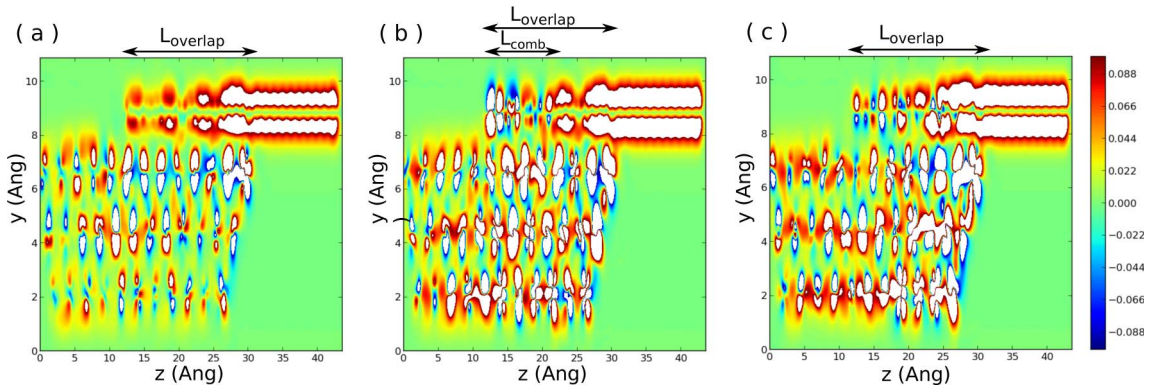


Fig. 13. Front view of the current density contour for (a) standard structure at 0 eV, (b) comb-shaped-contact structure at 0 eV, and (c) defected-contact structure at 0 eV.

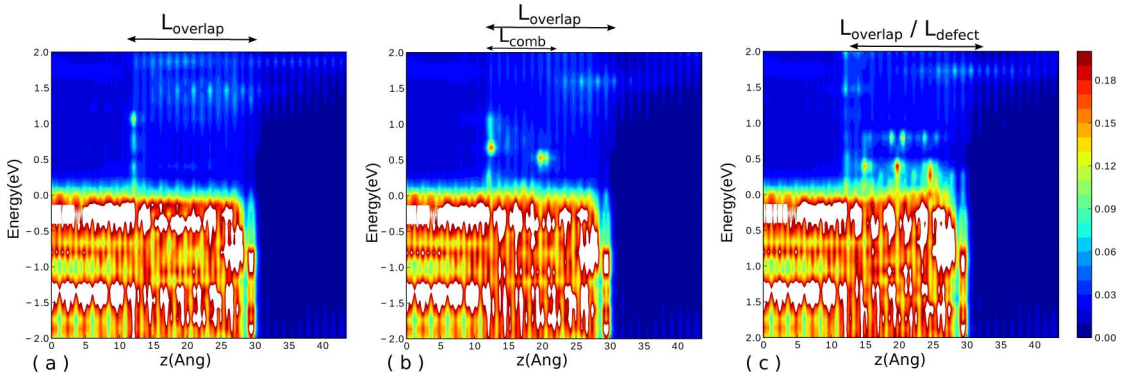


Fig. 14. LDOS of (a) standard structure, (b) comb-shaped-contact structure, and (c) defected-contact structure. The LDOS is averaged along the width of the palladium–graphene-contacted structures. (The regions marked in white are beyond the scale.)

are limited by the inability of carbon atoms in the interiors of the edge-contacted and sandwiched structures to form chemical covalent bond with the metal atoms. To increase the chemical bonding sites at the interface edge and reduce the contact resistance between metal and graphene, a novel way to create an interface is proposed in this section. Fig. 11(a)–(c) shows the top view of an standard contact, comb-shaped-contact geometry, and defected-contact geometry, respectively. A unique shape of the comb-shaped contact increases the number of sp-hybridized carbon atoms at the edge. Similarly, the defect creation in the overlap region by intentionally removing individual carbon atoms from the graphene plane increases the number of sp-hybridized carbon atoms within the graphene plane in the overlap region. A combination of both can maximize the sp-hybridized carbon atoms in the entire contact region.

*Ab-initio* calculations were conducted to compare the contact resistance of the three structures shown in Fig. 11. Fig. 12 shows an improvement of ∼20% for both comb-shaped-contact and defected-contact structures. To validate our initial guess, another structure with more comb teeth, i.e., increased sp-hybridized sites, was investigated. The calculated contact resistance was further reduced upholding the chemistry presented above. One may argue that increasing the edge transport might increase the current crowding [29]–[31] as majority of current flows through the graphene edge.

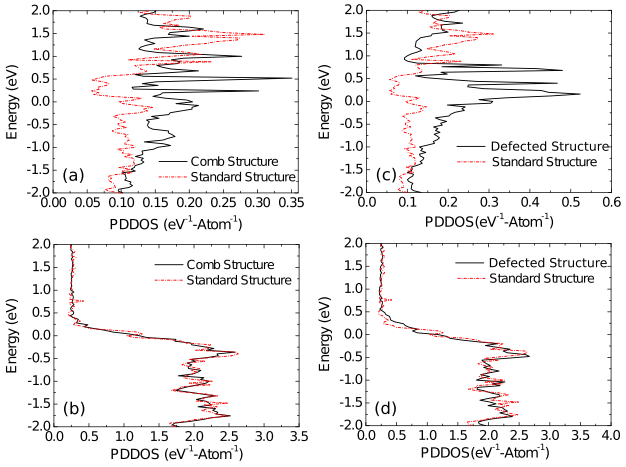


Fig. 15. PDDOS in standard and comb-shaped-contact structures for (a) graphene in the interface region and (b) palladium in the interface region. PDDOS in standard and defected-contact structures for (c) graphene in the interface region and (d) palladium in the interface region.

This can be resolved by increasing the defect sites in the overlap region and, hence, increasing the sp-hybridized carbon atoms.

The first cut view into the transport behavior of these geometries is given in Fig. 13 by investigating the current densities (without inclusion of nonlocal densities [32])

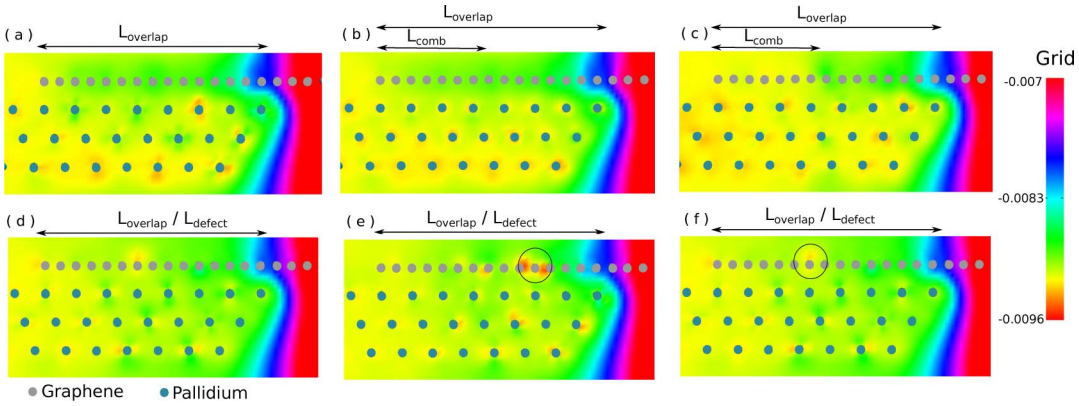


Fig. 16. Potential drop contours for (a) standard structure, (b) comb-shaped-contact structure with cut along BB′ [Fig. 11(b)], (c) comb-shaped-contact structure with cut along AA′ [Fig. 11(b)], (d) defected-contact structure with cut along XX′ [Fig. 11(c)], (e) defected-contact structure with cut along YY′ [Fig. 11(c)], and (f) defected-contact structure with cut along ZZ′ [Fig. 11(c)].

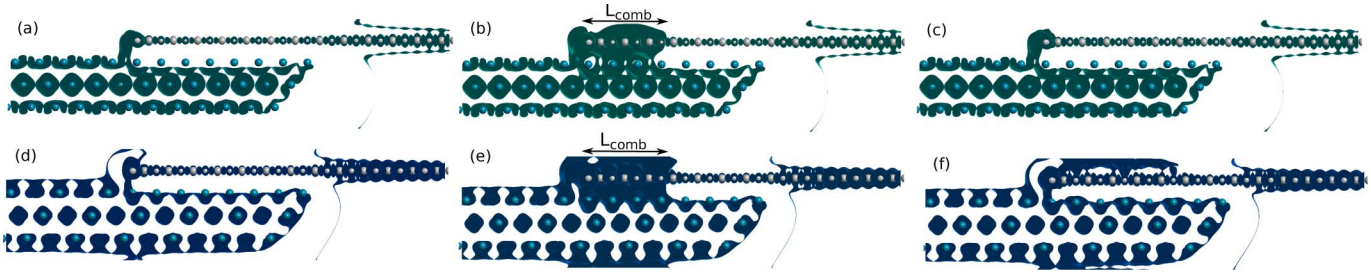


Fig. 17. Front view of electrostatic potential isosurface for (a) standard structure at 0.1 eV, (b) comb-shaped-contact structure at 0.1 eV, (c) defected-contact structure at 0.1 eV, (d) standard structure at −0.3 eV, (e) comb-shaped-contact structure at −0.3 eV and (f) defected-contact structure at −0.3 eV.

at 0 eV. The results shown in contour plot in Fig. 13 are real-space view of current density in the $yz$ plane. The current density in the graphene shows $\pi$-electrons carrying current symmetrically about the graphene sheet in the bulk region. There is a distinctive difference in the current densities among different structures depending upon the interfacing method. On comparison to the standard structure [Fig. 13(a)], comb-shaped and defected-contact geometries have high-current injection in the overlap regions [Fig. 13(b) and (c)].

LDOS and PDDOS, as shown in Figs. 14 and 15(a) and (c), show an improved graphene DOS for the comb-shaped and defected-contact structures unlike the standard-contact structure. On the other hand, the palladium DOS remains unchanged [Fig. 15(b) and (d)]. The increased DOS of graphene above Fermi energy in the comb or defected region is attributed to strong covalent bonding with palladium. The same does not change in the $sp^2$-hybridized regions due to lack of chemical bonding. Furthermore, to deduce the impact of the comb and defected geometries, the potential drop across various cross-sectional planes are studied, as shown in Fig. 16. In a nutshell, the maximum potential drop is observed in the edge or sp-hybridized regions, which validates the maximum charge transfer from these regions when compared with the $sp^2$-hybridized regions.

The spatial location of the transport channels is further validated using isosurface of the electrostatic potential for all the three contact geometries, as shown in Fig. 17. The isosurface of the electrostatic potential for the standard-contacted

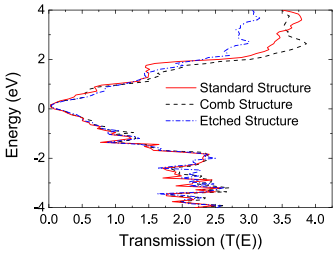


Fig. 18. Transmission spectrum for comb-shaped-contact, defected-contact, and standard-contact structures.

structure at 0.1 eV [Fig. 17(a)] as well as −0.3 eV [Fig. 17(d)] shows that the current predominantly flows only through the edge as the chemical bonds are formed only at the edge of the graphene sheet. However, in the comb-shaped contact, with chemically increased bonded region, the current flows through the entire comb region for both 0.1 eV [Fig. 17(b)] and −0.3 eV [Fig. 17(e)]. Similarly, the isosurface contour plot for the defected-contact structure, as shown in Fig. 17(c) and (f), shows the charge transfer from metal to graphene in the entire overlap region. The increased pathways for current injection, when compared with the standard structure [Fig. 17(d)], are clearly visible and are attributed to increase sp-hybridized sites.

So far, we have established that the contact resistance in comb and defected-contact geometries reduces due to an increased number of transport channels. However, one may

still ask whether or not the transmission probability improves with different contact geometries. Fig. 18 shows no change in the transmission spectrum. This validates that the contact resistance improvement in comb and defected-contact geometries is solely due to increased number of transport channels as created by increasing sp-hybridized sites over the contact region within the graphene plane.

## VII. Conclusion

Various contact geometries discussed and analyzed in this paper help in addressing the ambiguous behavior of the metal–graphene interface and chemical role of the metal–graphene interface. Role of sp-hybridized and $sp^2$-hybridized carbon atoms has discovered that the sp-hybridized sites at the edge of the graphene monolayer contribute to 40% of current conduction when compared with $sp^2$-hybridized atom sites in the graphene–metal overlap region. This is attributed to the increased number of transport channels due to strong covalent bonding between palladium atoms and sp-hybridized carbon atoms. We have also highlighted that the presence of an additional metal layer, i.e., the sandwiched contact, does not improve the chemical covalent bonding and, hence, the interface properties due to lacking sp-hybridized carbon sites. In fact for the sandwiched structure, a slight increase in resistance is observed, which can be attributed to the formation of chemical bond between some of the palladium atoms on either side of the graphene monolayer instead to the carbon atom in the graphene sheet. This paper for the first time has proposed a more fundamental way of defining the contact resistance, which is dependent on the nature of transport, bonding orbitals, and is given in units of per unit atoms. The edge region's contact resistance is calculated to be 1.28 $\mathrm{M}\Omega - atoms_{\mathrm{sp}}$. Similarly, the contact resistance per unit $sp^2$-hybridized carbon atoms has also been presented. Finally, the chemical role of sp-hybridized carbon atoms at the edge has suggested that increasing the sp-hybridized sites can potentially improve the contact resistance. To increase the chemical bonding sites at the interface edge and reduce the contact resistance between metal and graphene, comb-shaped-contact and defected-contact geometries are proposed, which together result in a 40% reduction in the contact resistance.

## Acknowledgment

M. Ghatge would like to thank the fellow scholars of the Advanced Nanoelectronic Device and Circuit Research Group for their fruitful and valuable discussions.

## References

[1] K. S. Novoselov *et al.*, "Electric field effect in atomically thin carbon films," *Science*, vol. 306, no. 5696, pp. 666–669, 2004.

[2] K. S. Novoselov, V. I. Fal'ko, L. Colombo, P. R. Gellert, M. G. Schwab, and K. Kim, "A roadmap for graphene," *Nature*, vol. 490, no. 7419, pp. 192–200, 2012.

[3] F. Bonaccorso, Z. Sun, T. Hasan, and A. C. Ferrari, "Graphene photonics and optoelectronics," *Nature Photon.*, vol. 4, no. 9, pp. 611–622, 2010.

[4] K. I. Bolotin *et al.*, "Ultrahigh electron mobility in suspended graphene," *Solid State Commun.*, vol. 146, nos. 9–10, pp. 351–355, 2008.

[5] C. Lee, X. Wei, J. W. Kysar, and J. Hone, "Measurement of the elastic properties and intrinsic strength of monolayer graphene," *Science*, vol. 321, no. 5887, pp. 385–388, 2008.

[6] G. Fiori and G. Iannaccone, "Insights on radio frequency bilayer graphene FETs," in *Proc. IEEE Int. Electron Devices Meeting*, Dec. 2012, pp. 17.3.1–17.3.4.

[7] I. Imperiale, S. Bonsignore, A. Gnudi, E. Gnani, S. Reggiani, and G. Baccarani, "Computational study of graphene nanoribbon FETs for RF applications," in *Proc. IEEE Int. Electron Devices Meeting (IEDM)*, Dec. 2010, pp. 32.3.1–32.3.4.

[8] J. Zheng *et al.*, "Sub-10 nm gate length graphene transistors: Operating at terahertz frequencies with current saturation," *Sci. Rep.*, vol. 3, Feb. 2013, Art. ID 1314.

[9] Y.-J. Yu, Y. Zhao, S. Ryu, L. E. Brus, K. S. Kim, and P. Kim, "Tuning the graphene work function by electric field effect," *Nano Lett.*, vol. 9, no. 10, pp. 3430–3434, 2009.

[10] K. Nagashio, T. Nishimura, K. Kita, and A. Toriumi, "Metal/graphene contact as a performance killer of ultra-high mobility graphene analysis of intrinsic mobility and contact resistance," in *Proc. IEEE Int. Electron Devices Meeting (IEDM)*, Dec. 2009, pp. 1–4.

[11] F. Xia, V. Perebeinos, Y.-M. Lin, Y. Wu, and P. Avouris, "The origins and limits of metal–graphene junction resistance," *Nature Nanotechnol.*, vol. 6, no. 3, pp. 179–184, 2011.

[12] L. Wang *et al.*, "One-dimensional electrical contact to a two-dimensional material," *Science*, vol. 342, no. 6158, pp. 614–617, 2013.

[13] Y. Matsuda, W.-Q. Deng, and W. A. Goddard, III, "Contact resistance for 'end-contacted' metal–graphene and metal–nanotube interfaces from quantum mechanics," *J. Phys. Chem. C*, vol. 114, no. 41, pp. 17845–17850, 2010.

[14] T. Chu and Z. Chen, "Understanding the electrical impact of edge contacts in few-layer graphene," *ACS Nano*, vol. 8, no. 4, pp. 3584–3589, 2014.

[15] Q. Gao and J. Guo, "Role of chemical termination in edge contact to graphene," *APL Mater.*, vol. 2, no. 5, p. 056105, 2014.

[16] A. D. Franklin, S.-J. Han, A. A. Bol, and V. Perebeinos, "Double contacts for improved performance of graphene transistors," *IEEE Electron Device Lett.*, vol. 33, no. 1, pp. 17–19, Jan. 2012.

[17] K. Stokbro, M. Engelund, and A. Blom, "Atomic-scale model for the contact resistance of the nickel-graphene interface," *Phys. Rev. B*, vol. 85, no. 16, p. 165442, 2012.

[18] T. Frederiksen, G. Foti, F. Scheurer, V. Speisser, and G. Schull, "Chemical control of electrical contact to $sp^2$ carbon atoms," *Nature Commun.*, vol. 5, Apr. 2014, Art. ID 3659.

[19] J. A. Robinson *et al.*, "Contacting graphene," *Appl. Phys. Lett.*, vol. 98, no. 5, p. 053103, 2011.

[20] W. S. Leong, C. T. Nai, and J. T. L. Thong, "What does annealing do to metal–graphene contacts?" *Nano Lett.*, vol. 14, no. 7, pp. 3840–3847, 2014.

[21] B. Ma, C. Gong, Y. Wen, R. Chen, K. Cho, and B. Shan, "Modulation of contact resistance between metal and graphene by controlling the graphene edge, contact area, and point defects: An *ab initio* study," *J. Appl. Phys.*, vol. 115, no. 18, p. 183708, 2014.

[22] Q. Ran, M. Gao, X. Guan, Y. Wang, and Z. Yu, "First-principles investigation on bonding formation and electronic structure of metal-graphene contacts," *Appl. Phys. Lett.*, vol. 94, no. 10, p. 103511, 2009.

[23] M. Brandbyge, J.-L. Mozos, P. Ordejón, J. Taylor, and K. Stokbro, "Density-functional method for nonequilibrium electron transport," *Phys. Rev. B*, vol. 65, no. 16, p. 165401, 2002.

[24] J. M. Soler *et al.*, "The SIESTA method for *ab initio* order-*N* materials simulation," *J. Phys., Condens. Matter*, vol. 14, no. 11, p. 2745, 2002.

[25] *QuantumWise ATK, Version 2014.0*, QuantumWise, Copenhagen, Denmark, 2014.

[26] M. J. Allen, V. C. Tung, and R. B. Kaner, "Honeycomb carbon: A review of graphene," *Chem. Rev.*, vol. 110, no. 1, pp. 132–145, 2009.

[27] P. E. M. Siegbahn, "Trends of metal-carbon bond strengths in transition metal complexes," *J. Phys. Chem.*, vol. 99, no. 34, pp. 12723–12729, 1995.

[28] T. Abtew, B.-C. Shih, S. Banerjee, and P. Zhang, "Graphene–ferromagnet interfaces: Hybridization, magnetization and charge transfer," *Nanoscale*, vol. 5, no. 5, pp. 1902–1909, 2013.

[29] K. Nagashio, T. Nishimura, K. Kita, and A. Toriumi, "Contact resistivity and current flow path at metal/graphene contact," *Appl. Phys. Lett.*, vol. 97, no. 14, p. 143514, 2010.

[30] A. D. Franklin, S.-J. Han, A. A. Bol, and W. Haensch, "Effects of nanoscale contacts to graphene," *IEEE Electron Device Lett.*, vol. 32, no. 8, pp. 1035–1037, Aug. 2011.
[31] H. Xu, S. Wang, Z. Zhang, Z. Wang, H. Xu, and L.-M. Peng, "Contact length scaling in graphene field-effect transistors," *Appl. Phys. Lett.*, vol. 100, no. 10, p. 103501, 2012.
[32] C. Li, L. Wan, Y. Wei, and J. Wang, "Definition of current density in the presence of a non-local potential," *Nanotechnology*, vol. 19, no. 15, p. 155401, 2008.

**Mayur Ghatge** received the B.Tech. degree in electrical engineering from IIT Jodhpur, Jodhpur, India, in 2014.

He then joined the Advanced Nanoelectronic Device and Circuit Research Laboratory, Indian Institute of Science, Bangalore, India, as a Research Assistant. His current research interests include 2-D-material-based device simulations focused on contact resistance.

**Mayank Shrivastava** (S'09–M'10) received Ph.D. degree from the Indian Institute of Technology Bombay, Mumbai, India, in 2010.

He is currently an Assistant Professor at the Indian Institute of Science, Bangalore, India. He is the recipient of the 2015 IEEE EDS Early Career Award. He has over 45 publications in international journals/conferences, and holds 25 patents. His research interest broadly covers nanoelectronics/nanotechnological solutions for system-on-chip and system-on-board applications, and on-chip ESD and power semiconductor devices.